Electronic Supplementary Material (ESI) for Nanoscale.

Supporting Information

Cable-like Heterogeneous Porous Carbon Fibers with Ultrahigh-Rate Capability and Long Cycle Life for Fast Charging Lithium-Ion Storage Devices

Yuan Zhang, Mutian Zhang, Wei Liu, Yongpeng Cui, Tianqi Wang, Shuang Liu, Huanlei Wang, Shougang Chen, Minghua Huang, Yongxu Du*

School of Materials Science and Engineering, Ocean University of China, Qingdao 266100, China.

Email: weiliu@ouc.edu.cn (W. Liu)

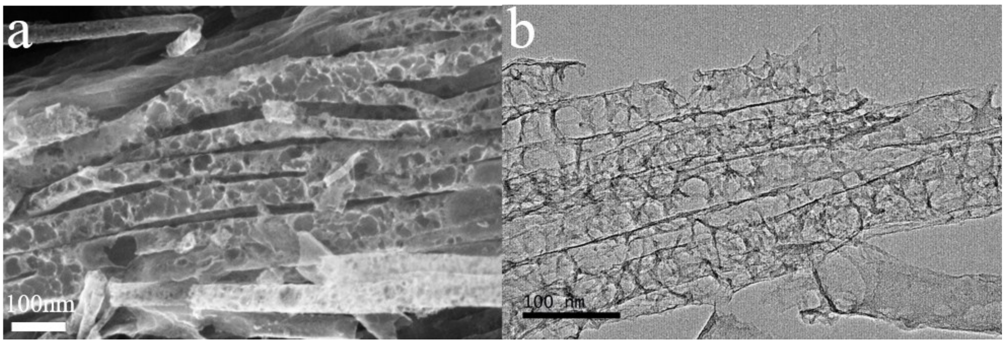

Figure S1. (a-b) SEM and TEM images of Si-CPCF sample.

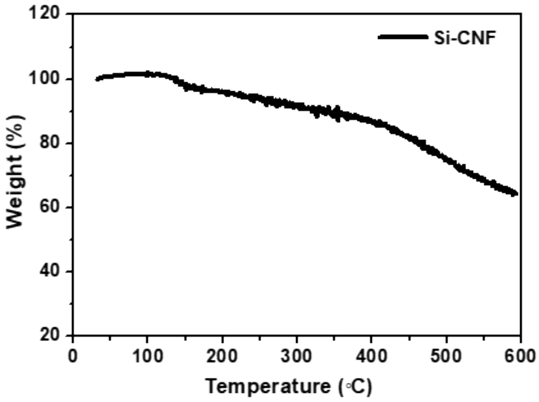

Figure S2. TG curve of the precursor of the Si-CNF sample in N_2 atmosphere.

The first weight loss at 110-400 ℃ can be ascribed to the partly volatilization of TEOS and the pre-carbonation of resin, and then follows another weight-loss step at 400-600 ℃ can be mainly attributed to the carbonation of TEOS and resin. Due to the barrier of crab shell, the residual TEOS was left in carbon fibers and pyrolysized to Si elements, leading to the Si-doping in carbon fibers. The corresponding SEM-EDX results of the cross-section part of carbon fibers prepared in capillary glass tube also confirmed this process.

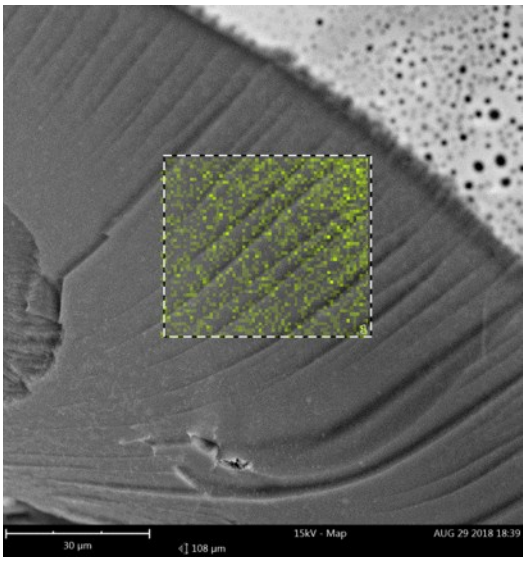

Figure S3. SEM of the cross-section of carbon fiber prepared by using capillary glass tube and EDX elemental mapping images of Si (inset picture).

The Si-CPCF nanofibers are very fine (about 70 nm), which is difficult to find out their cross section image by TEM observation. Therefore, we used capillary glass tube to simulate the nanotube structure of the crab shell. The resin with TEOS was poured into capillary tube and then cured and calcined. The cross-section of the obtained carbon fiber was observed by using SEM. As shown in Figure S3, silicon was enriched on the surface of the obtained carbon fiber. The EDX image (inset) visually reflected the gradient distribution of silicon from the inside to the outside, which proved the uneven distribution of doped Si atoms in the Si-CPCFs to some extent.

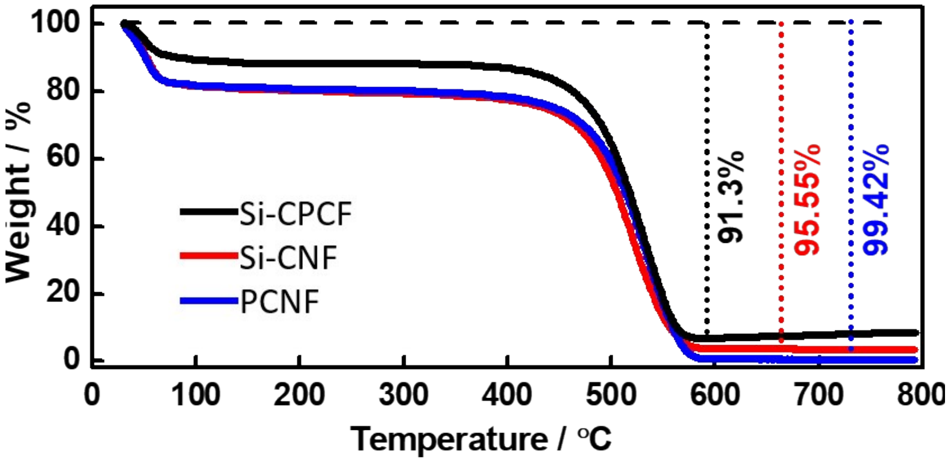

Figure S4. TG curves of Si-CPCF, Si-CNF, and PCNF in air atmosphere.

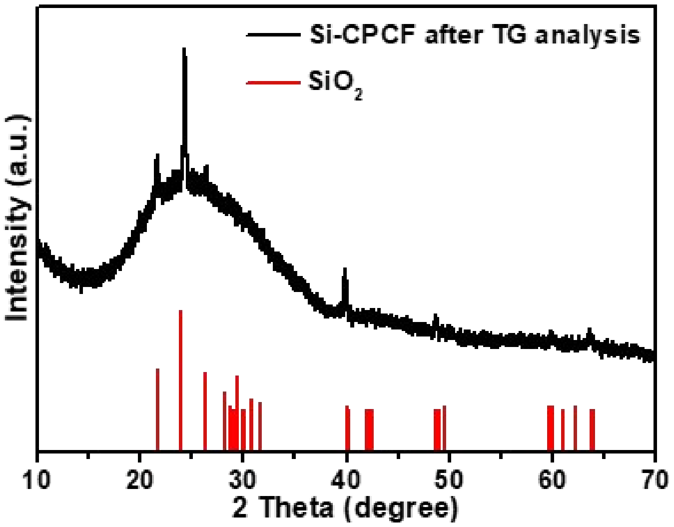

Figure S5. XRD of Si-CPCF after TG analysis.

As shown in Figure S4, the residual mass of Si-CPCF after calcination in air was 8.7%. The XRD result of the residue of TG analysis (Figure S5) showed that the product was basically SiO_2. As a result, the residual mass ratio of Si was about 4.06%, and the atomic ratio was 1.8%.

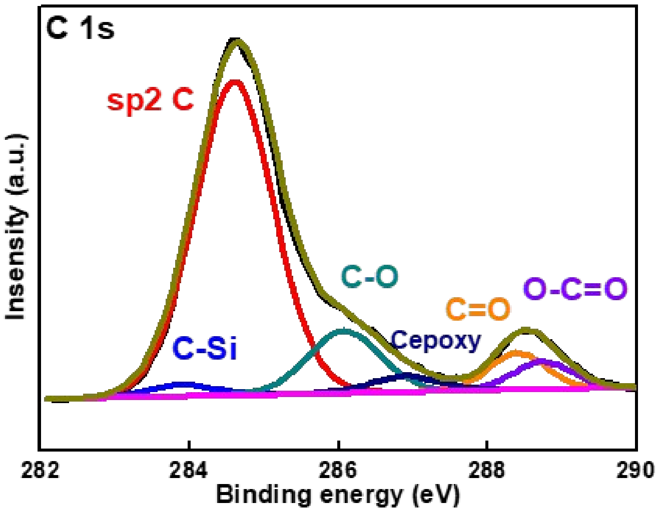

Figure S6. C 1s XPS spectra and fitting peaks curves of Si-CPCF.

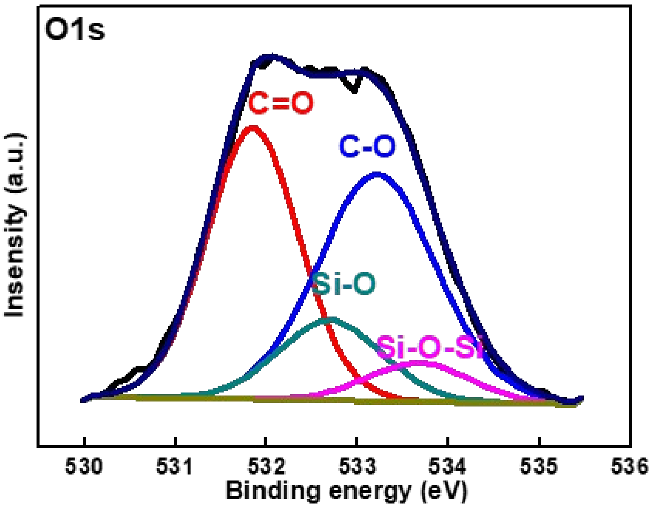

Figure S7. XPS O 1s spectra and fitting peaks of the Si-CPCF.

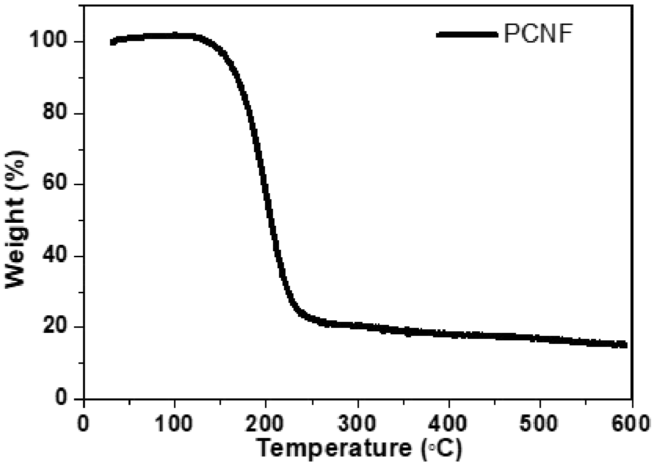

Figure S8. TG curve of the precursors of PCNF in N_2 atmosphere.

During the heating process, the volatilization of TBP in the PCNF sample give rise to the weight loss in the temperature range from 100℃ to 250℃. During this temperature range, the resin was changed to viscous liquid. As a result, the volatilization of TBP gives rise to the foaming in the resin, which were fixed in cured resin fibers to produce numerous pores.

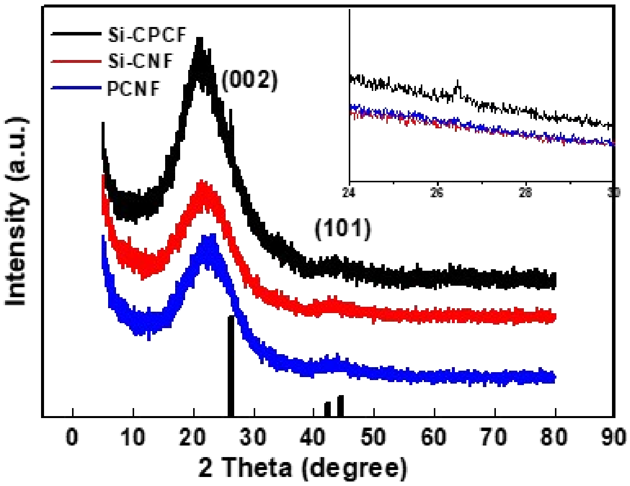

Figure S9. XRD comparison of Si-CPCF, Si-CNF and PCNF. The inset image is the partially magnified XRD pattern between 24°-30°.

Table S1. Comparison of Si-CPCF with typical carbon-based anode materials.

Material	**Current (A g^{-1})**	**Capacity (mAh g^{-1})**	**Current (A g^{-1})**	**Capacity (mAh g^{-1})**	**Capacity (mAh g^{-1}) (Current (A g^{-1}),Cycles)**	**Ref**
0.1-BNC	5	375	10	272	450 (2,5000)	Ref1
NFG-150	5	305	——	——	295 (5, 2000)	Ref2
NGM	3.72	180	——	——	1078 (0.359,350)	Ref3
N-doped graphene	5	290	30	~80	~100 (20, 2000) ~50 (30,2000)	Ref4
Graphene	5	275	——	——	556 (1, 300)	Ref5
PNCG-600	7.44	~300	——	——	318 (7.44,6000)	Ref6
ANHTGCNs	5	495	10	380	~200 (10, 2000)	Ref7
N7.8%-aC$_{60}$	5	600	——	——	300 (5, 2000)	Ref8
N-doped CNT	1.488	363	——	——	320 (1.488,400)	Ref9
HPNC-600	5	470	——	——	396 (5,1000)	Ref10
Laser-scribed graphene paper	1.86	335	55.8	~60	150 (14.8, 1000) ~61 (55.8,6000)	Ref11
CNS	5	400	20	240	415 (5,1300)	Ref12
NOSDCA-3	5	~270	10	228	488 (1,500)	Ref13
Si-CPCF	**5**	**381**	**50** **100**	**260** **170**	**322 (10, 5000)** **132 (100, 10000)**	**This work**

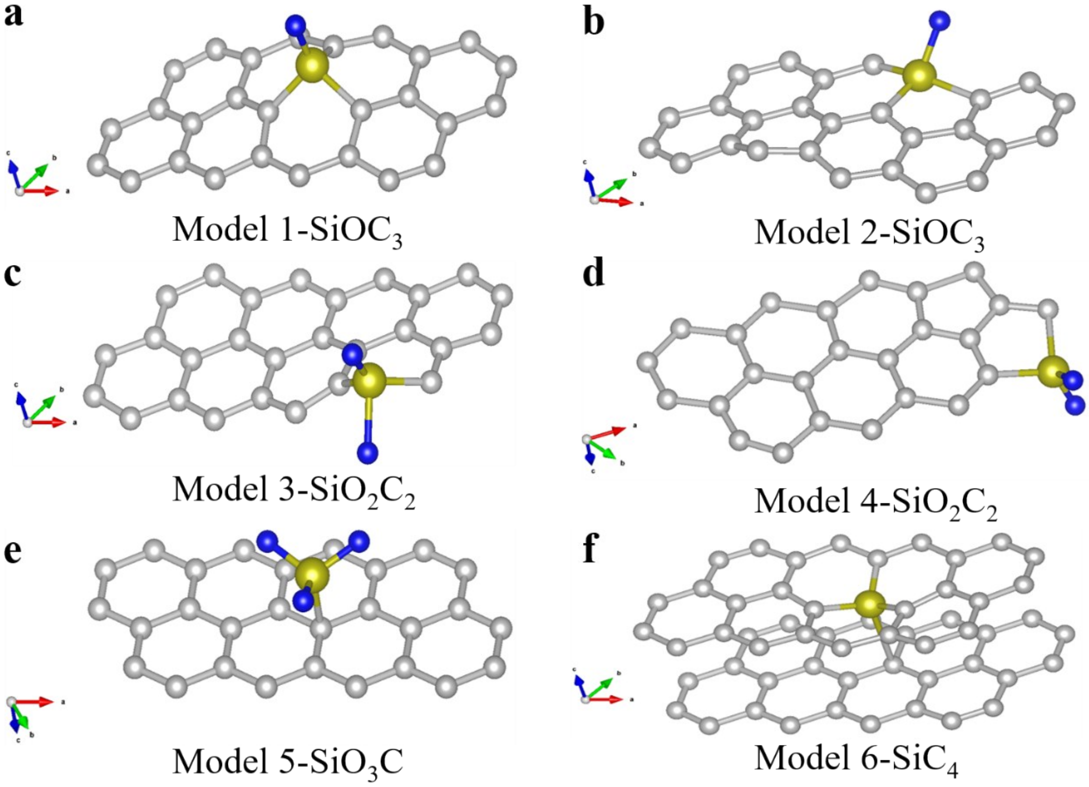

Model 1-$SiOC_3$
Model 2-$SiOC_3$
Model 3-SiO_2C_2
Model 4-SiO_2C_2
Model 5-SiO_3C
Model 6-SiC_4

Figure S10. (a-f) Schematic illustration of six models for Si doped configurations in sp2 carbon plane before optimization.

Table S2. The bound energy of six models

	E_{total}(eV)	**E_1(eV)**	**E_2(eV)**	**E_b(eV)**
Model1	-8606.800	-8494.860	-101.902	-10.038
Model2	-5037.462	-4489.224	-542.884	-5.354
Model3	-4882.365	-4330.613	-542.874	-8.878
Model4	-6064.390	-4652.568	-1412.449	0.627
Model5	-5319.508	-4332.354	-975.202	-11.952
Model6	-5005.196	-4016.443	-973.010	-15.473

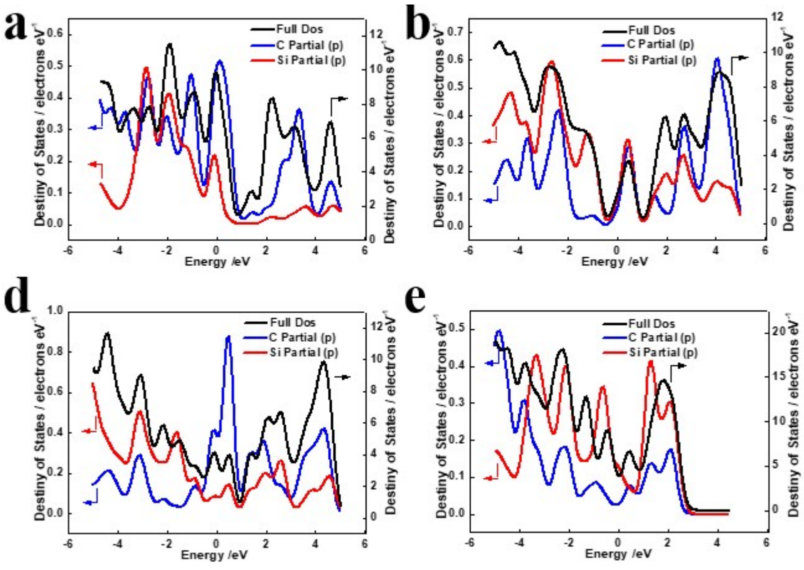

Figure S11. (a-e) P orbital electron density of state for Si, C and full DOS of model 1, 2, 3, 5, 6.

Table S3 Bond length of five models

Model	Bond length (nm)	Compare with SiC(%)
Model1	0.18185	-3.78
Model2	0.18685	-1.14
Model3	0.18059	-4.45
Model5	0.18481	-2.22
Model6	0.20048	6.07

In this study, the structure was calculated using the density functional theory (DFT)-based CASTEP software package, and the GGA-PBE type exchange correlation functional was used. The interaction between atoms was simulated using the ultra-soft pseudopotential method. The CASTEP software package requires that the computing system must have periodicity, and our structure can be considered to have some periodicity in the plane. When optimizing the structure, the interlayer spacing is set to 2.04 nm in the lattice parameters to establish periodic crystal cells, which can ignore the role of the nearest neighbor graphene layers. The BFGS optimization algorithm is used for geometric optimization. After convergence test, the cut-off energy is set to 340 ev, and the k-point in the brillouin zone is set to 3*5*1 to satisfy the reciprocal spatial geometry relationship. The structure is optimized for geometry and performance is calculated. The possible Si dopant configuration in carbon planes were investigated by DFT calculations. As shown in **Figure S10**, six models of Si doped configurations in sp2 carbon plane were constructed. In order to prove the existence of a stable model, the bound energy (Eb) is defined as Equation (1):

$$E_b = E_{total} - E_1 - E_2 \qquad (1)$$

Where E_{total} is the total energies of the system, E_1 is the energy of the graphene and E_2 is the energy of Si-O in such structure. The lower the binding energy is, the more stable the structure is. There are no stable structures when the E_b values are positive. The **Table S2** reveals the bound energy of the six models, the model 4 was proved as an unstable structure because of its positive E_b value. In **Figure S11**, there is a high degree of coincidence of P orbital electron density of state for Si, C for the Model 1, 2, 3, as well as the coincident peaks can find in the full DOS. It's a strong evidence for Si-C bonding stably.

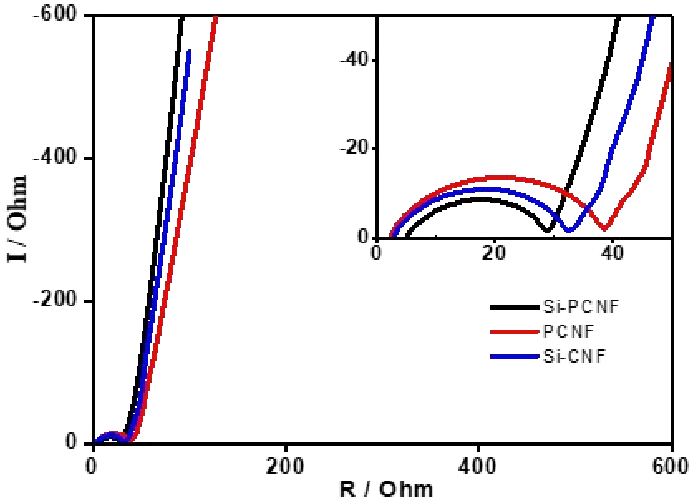

Figure S12. Electrochemical impedance spectra of all samples.

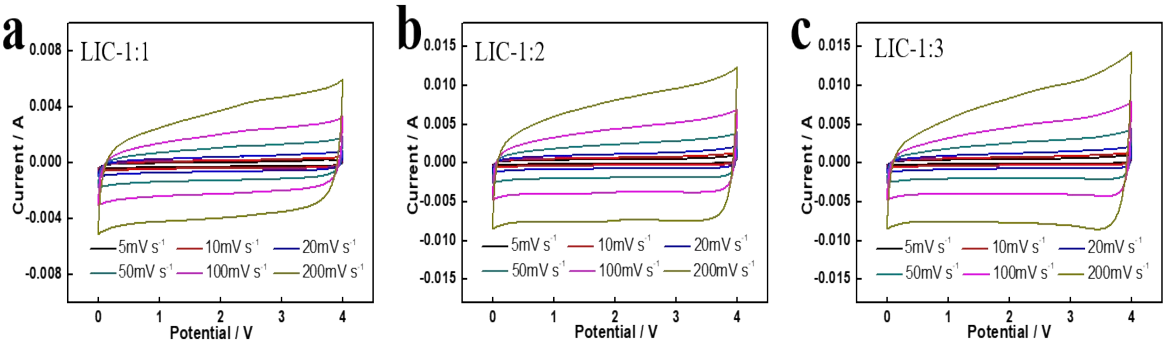

Figure S13. (a-c) CV curves of all the devises at different scan rates.

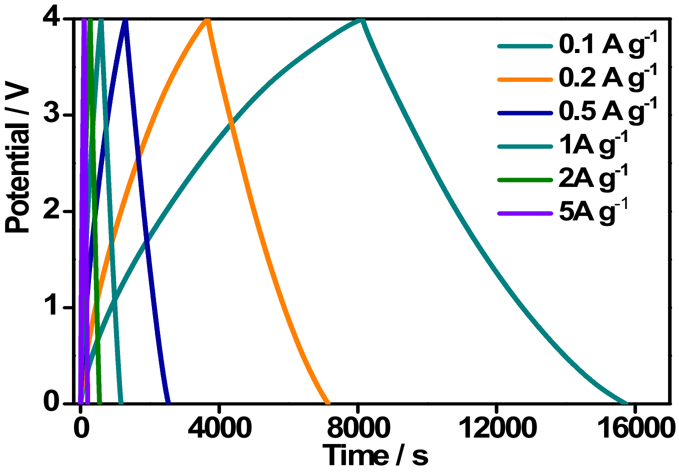

Figure S14. Charge-discharge curves of of the LIHC with a 1:2 ratio.

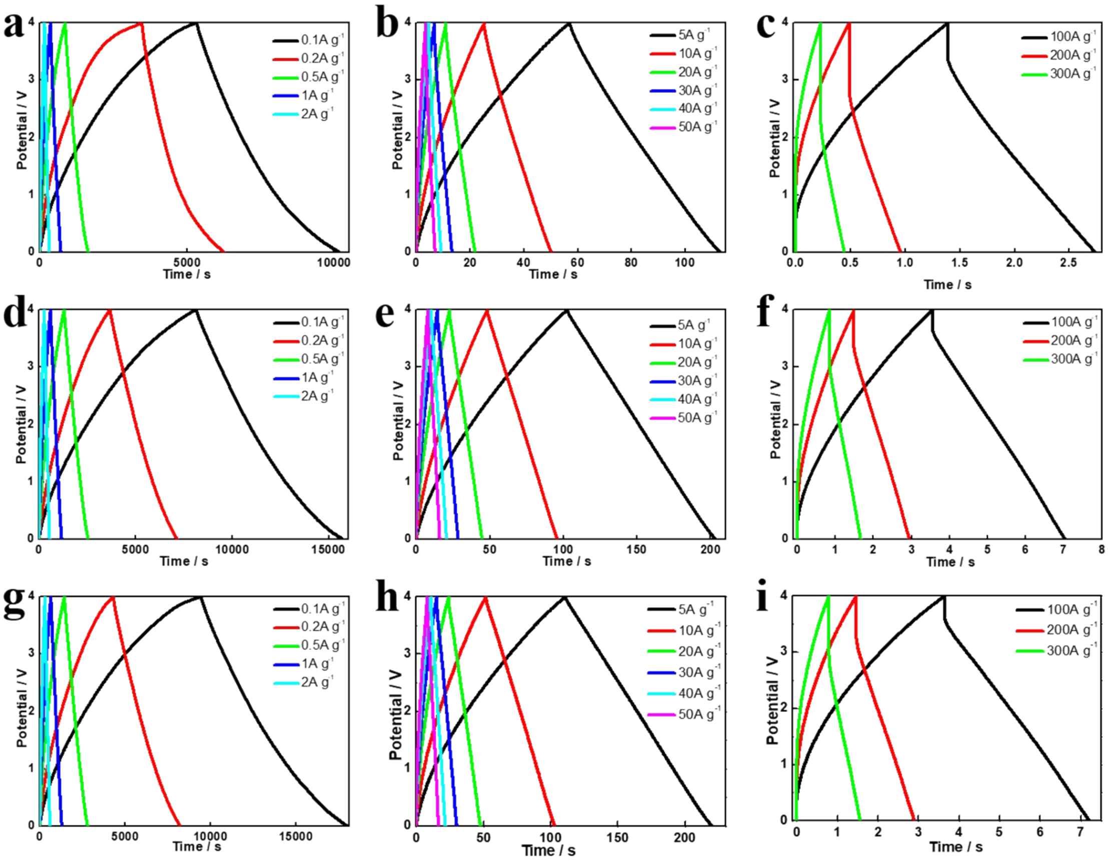

Figure S15. Typical charge-discharge curves of (a-c) LIC-1:1; (d-f) LIC-1:2; (g-i) LIC-1:3 at different current densities of 0.1-300 A g^{-1} for the voltage window of 0-4.0 V.

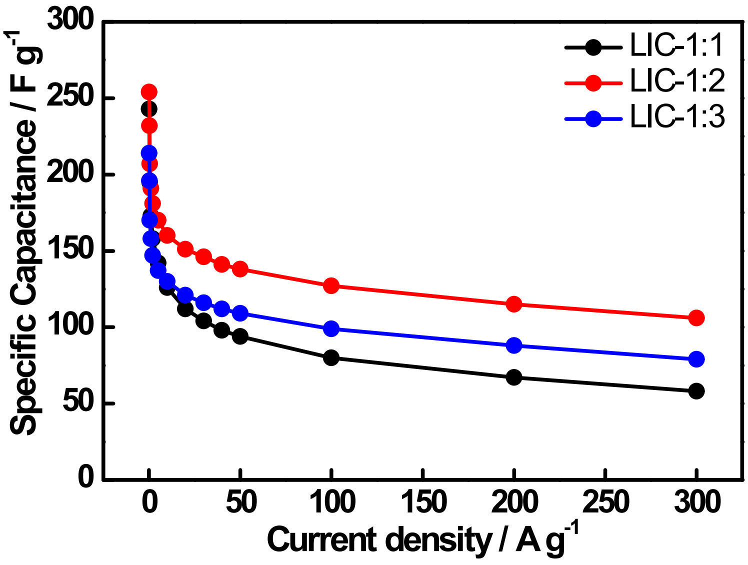

Figure S16. Specific capacitance of the devises at different current densities based on total mass of the both cathode and anode.

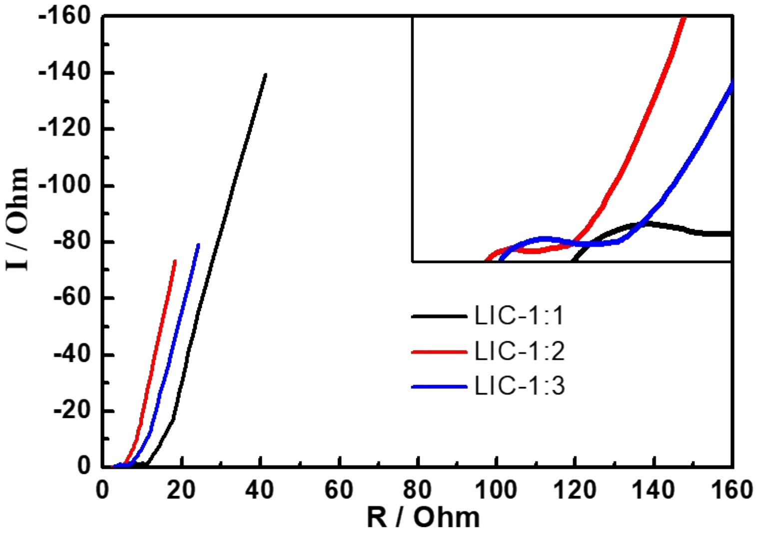

Figure S17. Nyquist plots with various anode/cathode mass ratios.

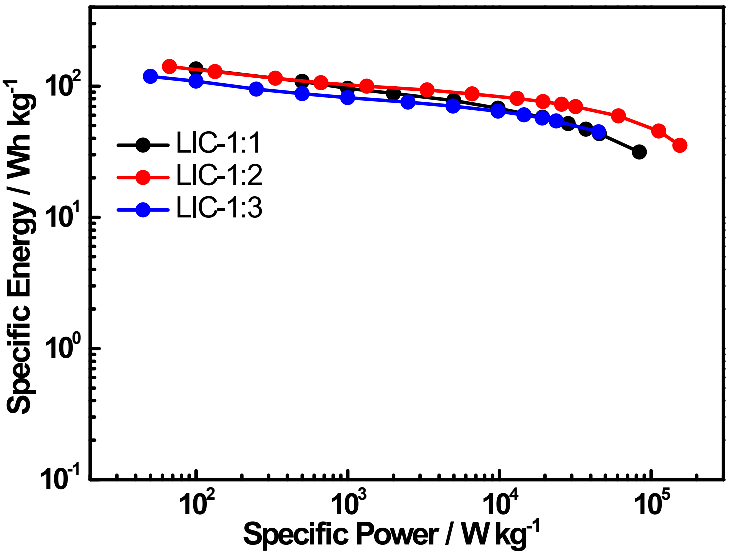

Figure S18. Ragone plots of Si-CPCF//NPC LIHCs with different anode to cathode mass ratios.

References

1. Q. Xia, H. Yang, M. Wang, M. Yang, Q. Guo, L. Wan, H. Xia, Y. Yu, Adv. Energy Mater. 7 (2017) 1701336.
2. S. Huang, Y. Li, Y. Feng, H. An, P. Long, C. Qin, W. Feng, J. Mater. Chem. A 3 (2015) 23095-23105.
3. Z. Du, W. Ai, C. Sun, C. Zou, J. Zhao, Y. Chen, X. Dong, J. Liu, G. Sun, T. Yu, W. Huang, ACS Appl. Mater. Interfaces 8 (2016) 33712-33722.
4. T. Hu, X. Sun, H. Sun, G. Xin, D. Shao, C. Liu, J. Lian, Phys. Chem. Chem. Phys. 16 (2014) 1060-1066.
5. D. Cai, S. Wang, L. Ding, P. Lian, S. Zhang, F. Peng, H. Wang, J. Power Sources 254 (2014) 198-203.
6. J. Gu, Z. Du, C. Zhang, S. Yang, Adv. Energy Mater. 6 (2016) 1600917.
7. Y. Chen, X. Li, X. Zhou, H. Yao, H. Huang, Y.-W. Mai, L. Zhou, Energy Environ. Sci. 7 (2014) 2689-2696.
8. Z. Tan, K. Ni, G. Chen, W. Zeng, Z. Tao, M. Ikram, Q. Zhang, H. Wang, L. Sun, X. Zhu, X. Wu, H. Ji, R.S. Ruoff, Y. Zhu, Adv. Mater. 29 (2017).
9. Z. Pan, J. Ren, G. Guan, X. Fang, B. Wang, S.-G. Doo, I.H. Son, X. Huang, H. Peng, Adv. Energy Mater. 6 (2016) 1600271.
10. L. Ma, R. Chen, Y. Hu, G. Zhu, T. Chen, H. Lu, J. Liang, Z. Tie, Z. Jin, J. Liu, Nanoscale 8 (2016) 17911-17918.
11. R. Mukherjee, A.V. Thomas, Ajay Krishnamurthy, A.N. Koratkar, ACS Nano 6 (2012) 7867-7878.
12. Y. Chen, L. Shi, S. Guo, Q. Yuan, X. Chen, J. Zhou, H. Song, J. Mater. Chem. A 5 (2017) 19866-19874.
13. M. Lu, W. Yu, J. Shi, W. Liu, S. Chen, X. Wang, H. Wang, Electrochim. Acta 251 (2017) 396-406.